Applied Catalysis B: Environmental 180 (2016) 416–423

Contents lists available at ScienceDirect

Applied Catalysis B: Environmental

journal homepage: www.elsevier.com/locate/apcatb

Preparation and photocatalytic performance of transparent titania film from monolayer titania quantum dots

Hanyang Gao [a], Wenfeng Shangguan [a,*], Guoxin Hu [b], Kunxu Zhu [b]

[a] Research Center for Combustion and Environment Technology, Shanghai Jiao Tong University, 800 Dongchuan Road, Shanghai 200240, China
[b] School of Mechanical and Power Engineering, Shanghai Jiao Tong University, 800 Dongchuan Road, 200240 Shanghai, China

ARTICLE INFO

Article history:
Received 4 May 2015
Received in revised form 23 June 2015
Accepted 25 June 2015
Available online 2 July 2015

Keywords:
Titania quantum dots
Ultrathin film
Graphene
Photocatalytic performance
Coffee-ring effect

ABSTRACT

By using monolayer titania quantum dots (MTQDs) colloid, a continuous and transparent ultrathin titania film was prepared simply by drop-cast or spray coating method at room temperature. The formation of this even and ultrathin film was not only because of the very thin thickness of two-dimensional MTQDs, but also because of the suppression of coffee-ring effect. The self-assembly behaviors of MTQDs were examined by AFM and the reason for the suppression of coffee-ring effect was discussed in detail. Furthermore, the photocatalytic performance of this MTQDs film was evaluated and an improvement was achieved by loading graphene. Comparison between MTQDs/graphene composite and sphere-shaped nanoTiO_2/graphene composite indicated that, the face-to-face contact mode between MTQDs and graphene may contribute to the high activity of MTQDs/graphene composite.

1. Introduction

Owing to the inherent excellent photocatalytic, photoelectrical properties, and chemical stability, titania film has been proven as a high efficiency, environmental friendly catalytic film, and can be applied to various applications, such as antibacterial coating, antifogging coating, self-cleaning film, deodorant fiber, gas sensors, photovoltaic devices, and photocatalysis [1–3]. Well-crystallized titania coatings can be prepared by multiple deposition techniques, such as sol–gel [4], sputtering [5], and spray pyrolysis [6]. Since crystalline degree of catalysts strongly affect their catalytic activity, a heating treatment at relatively high temperatures above 400 °C is usually required to obtain sufficient crystallinity in these methods. During the heating process, along with crystallinity, catalyst particles unavoidably grow and aggregate [7], making it difficult to produce an ultrathin and transparent highly crystalline titania film.

In our previous study, monolayer titania quantum dots (MTQDs) with two-dimensional morphology and ~0.4 nm thickness were synthesized by treating titania nanotubes (TNTs) in supercritical water (SCW) [8]. The high crystallinity and special plane morphology of MTQDs, may give us an opportunity to prepare an ultrathin and transparent titania film at room temperature. Furthermore, because MTQDs and graphene both possess a plane morphology, it can be expected that the combination of MTQDs and graphene will in a plane–plane mode instead of a point-plane mode. The enlargement of contact area will be beneficial for electronic transfer, and therefore will facilitate the photocatalytic performance of the composites. It also can be expected that comparing with the combination between sphere-shape TiO_2 particles and paper-like graphene, the stacking of two kinds of two-dimensional particles has more tendency to form a smooth film with ultrathin thickness.

In this article, based on our previous study, the self-assembly behavior of MTQDs was observed by AFM. Taking advantage of the special assembly behaviors of MTQDs, a highly crystallized, ultrathin, and transparent titania film was prepared using MTQDs colloid at room temperature by a simple drop casting method. The photocatalytic performance of the self-assembly film with or without graphene enhancement was discussed. The effect of the special face-to-face contact mode between MTQDs and graphene (which possessing similar two-dimensional morphology) on photocatalytic efficiency was compared with the effect of common point-to-face contact mode between sphere-shaped TiO_2 particles and graphene. To our knowledge, this is the first time to report the self-assembly behavior of the very tiny two-dimensional titania nanosheets and the further thin-film fabrication from them. The comparison of the effect of two different contact modes between titania particles and graphene on photocatalytic efficiency may also provide some useful information for the development of graphene-based composite catalyst.

* Corresponding author. Fax: +86 21 34206020.
E-mail address: shangguan@sjtu.edu.cn (W. Shangguan).

http://dx.doi.org/10.1016/j.apcatb.2015.06.049
0926-3373/

2. Materials and methods

All the reaction in SCW was carried out in a 15 mL SCHOELLER 316L SS stainless-steel reactor (caution: the reactor maximum loading is 80% (12 mL), the remaining space is filled with air). All reagents were analytical grade and used without any further purification.

2.1. Synthesis of TNTs

As precious reports [9,10], to prepare the TNTs, 2 g commercially available anatase TiO_2 powder (Aladdin, Shanghai) was added in 70 mL 10 M NaOH aqueous solution, the mixture was then held at 130 °C in a 100 mL Teflon-lined autoclave for 10 h. After the alkali treatment, the autoclave cooled down naturally to room temperature. The resulting sample was washed with 0.1 M HCl and then with de-ionized water until a pH value near 7 was reached. After filtered and dried in the drying oven at 60 °C for 24 h, the TNTs white powder was obtained.

2.2. Synthesis of MTQDs

MTQDs were synthesized by treating TNTs in SCW as reported in our previous study [8]. In a typical procedure, 25 mg as-prepared TNTs powder and 10 mL de-ionized water were mixed and dispersed with ultrasonic agitation (40 kHz, maximum output power 180 W) for 15 min, and then carefully transferred into the reactor. The reactor was sealed and heated in a tube furnace at 400 °C for 20 min, then was cooled rapidly in ice water. The products were transferred into a beaker and dispersed by sonication for 5 min. The resulting solution was further dialyzed in a dialysis bag (retained molecular weight 2000 Da) for 24 h to obtain the MTQDs colloid (see Refs. [8] and [11] for more information.).

2.3. Synthesis of graphene in SCW

The procedure of graphene producing in supercritical fluid was described in our previous research in detail [12]. Typically, expandable graphite powder (Qingdao Tianhe Graphite Co., Ltd., China) was added in DMF (Sinopharm Chemical Reagent Co., Ltd.) and dispersed by sonication for 15 min, and then transferred into the stainless-steel reactor. The reactor was sealed and heated in a tube furnace at 400 °C for 30 min, then was cooled rapidly in ice water. The obtained production was centrifuged in 6000 rpm for 10 min, suspension was then filtered through film (PVDF) and washed several times with fresh solvent. The resulting products were vacuum dried overnight at 100 °C to obtain graphene.

2.4. Synthesis of graphene/MTQDs composite

To prepare graphene/MTQDs suspension, MTQDs colloid and graphene were mixed together in different proportions and sonicated for 15 min to obtain stable composite colloid. After filtration and drying, graphene/MTQDs particles were obtained.

2.5. Synthesis of sphere nanoTiO$_2$ and nanoTiO$_2$/graphene composite

Based on our previous report [13], 5 mL $Ti(OBu)_4$ (Sinopharm Chemical Reagent Co., Ltd.) and 1 mL PrOH were added in 50 mL de-ionized water and kept under reflux condition at 75 °C for 24 h to obtain nanoTiO$_2$ colloid. The as-prepared nanoTiO$_2$ colloid was subject to dialysis in water to remove the residual PrOH. For preparing nanoTiO$_2$/graphene colloid, graphene solution instead of pure de-ionized water was add in for the reflux treatment. After flocculation, filtration, and drying, the composite particles were obtained.

2.6. Material characterization

The surface morphology was examined by a JEM-2100F high resolution-transmission electron microscope (HRTEM) operated at 200 kV with a point-to-point resolution of 0.19 nm. Atomic force microscopy (AFM) measurements were carried out with an E-sweep/NanoNavi Station (SII Nanotechnology, Inc., Tokyo, Japan). The resistant measurement was performed by a Honeytek DT9205 digital multimeter. Transient photocurrents test was performed on a CHI660C electrochemical workstation (Chenhua Instruments Co., Shanghai, China).

2.7. Photocatalytic performance test

Dye concentration in the aqueous solution after irradiation was measured by a SHIMADZU UV-2450 spectrophotometer. Catalyst/dye solution was irradiated with a 350 W Xe-lamp.

3. Results and discussion

3.1. Morphology and structure of MTQDs

While temperature and pressure get to the critical point of water, wide-range hydrogen bonding network breaks down into small water clusters which possess special characteristics such as

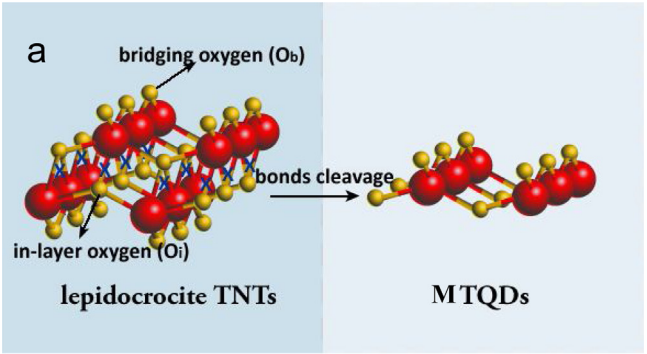

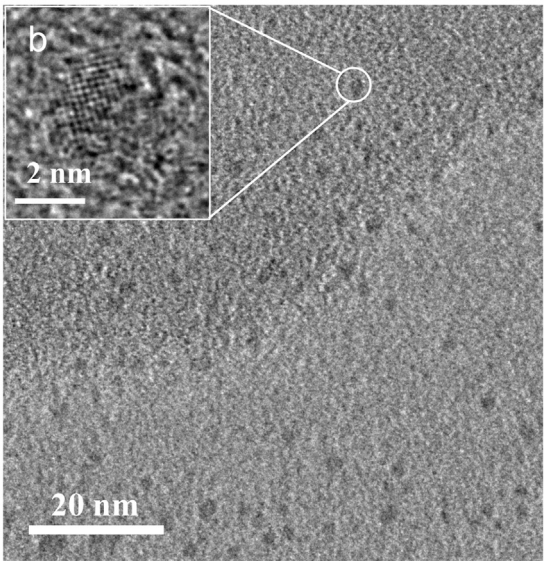

Fig. 1. (a) Chemical structure of lepidocrocite TNTs and MTQDs. (b) TEM and HRTEM images of discrete MTQDs.

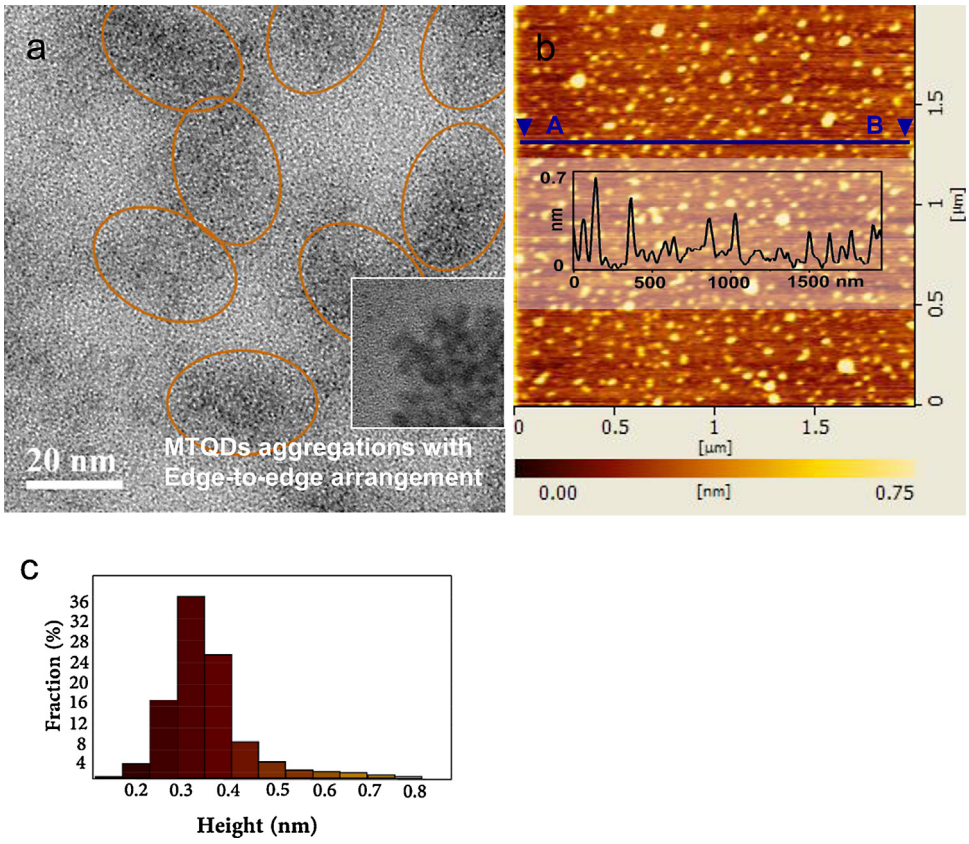

Fig. 2. (a) The TEM image of the aggregated MTQDs. Inset: enlarged view of MTQDs aggregation, (b) AFM image and (c) height distribution of MTQDs aggregations.

high self-diffusivity, high solvating power, low interfacial tension, and high diffusion coefficient. Meanwhile, the concentrations of both H^+ and OH^- are about three orders of magnitude higher than that in ambient water [14,15]. Therefore, at this condition, SCW can be considered to be both acidic and alkaline, and play the role of an acid or base catalyst precursor [16].

The growth mechanism and structure of MTQDs are studied in our previous research in detail [8]. In short, view along [0 0 1] direction, TNTs lepidocrocite sheets can be considered as being constituted by bilayer TiO6 slabs with the upper slab slide half a unit cell over the lower one [17]. The thickness of TNTs sheets is around 0.75 nm [17–19]. Two types of oxygen atoms, two-coordinated bridging oxygen atoms (O_b) and four-coordinated inlayer (O_i) oxygen atoms, exist in lepidocrocite TNTs (Fig. 1a). Because the bond length of O_b—Ti (1.813 Å) is shorter than that of O_i—Ti (1.966 Å and 2.174 Å) [20], O_i—Ti bonds have a lower energy and are more easier to be cut off. During the SCW process, at the beginning, both O_i—Ti and O_b—Ti bonds of TNTs are ruptured by the high temperature, high pressure, and high H^+/OH^- concentration of SCW, large lepidocrocite TNTs sheets crack into small fragments and bilayer slabs dissolve into monolayer. Meanwhile, along with cracking and dissolving, big sheets are broken into smaller pieces, the length of O_b—Ti bonds in the fragments become shorter and the interactions within planar enhance gradually [21]. When lateral size of the fragments is reduced to around 2 nm, the bond energy in (0 0 1) planar becomes big enough to withstand the external destructive force, destructions stops and the structure of MTQDs is maintained (Fig. 1a).

To examine the morphology, a drop of MTQDs colloid with low concentration is deposited on an ultrathin amorphous carbon grid for the detection of TEM (~0.2 mg/L, dried at 90% ambient humidity, 10 °C). TEM images show that the lateral dimension of typical discrete MTQDs (Fig. 1b) is about 2–3 nm. HRTEM images (inset, Fig. 1b) show clear lattice fringes, demonstrating that the MTQDs are highly crystallized. Furthermore, it can be noticed from the images that, at this concentration and drying condition, apart from a few discrete particles, most MTQDs particles tend to aggregate together to form many small rafts with lateral size around 20–30 nm (Fig. 2a). Similar MTQDs aggregations can also be observed in AFM detection (Fig. 2b). Height distribution diagram and thickness profile show that the thickness of these MTQDs aggregations is mainly distributed at 0.3–0.4 nm (Fig. 2c). Because the thickness of MTQDs is about a half of that of protonic TNTs, it can be deduced from height distribution diagram that the MTQDs detected in TEM and AFM are aggregated in an edge-to-edge arrangement, similarly with the self-assembly behavior of hexabenzocoronene (HBC) molecules which have analogous platelet morphology [22].

3.2. *MTQDs film formation in drop casting process*

Because of the ultrathin thickness and special two-dimensional morphology of MTQDs, they are likely to self-assemble into an ultrathin and transparent titania film. In consideration of the very small size of MTQDs, AFM is used to observe the self-assembly behavior of MTQDs. A drop of 0.1 mL MTQDs colloid with different concentration (0.5 mg/L, 0.2 mg/L, 1 mg/L, and 5 mg/L) is deposited on a mica substrate and dried under controlled condition (ambient humidity 90%, temperature 10 °C).

From AFM images (Fig. 3a and b) of dried MTQDs with a concentration of 0.5 mg/L, the tendency of MTQDs particles to gather and bind together can be clearly seen. Many small MTQDs rafts formed in the initial stage of drying process assemble together to form a large domain. The bindings between rafts are close and tight. Different from the edge-to-edge assembly mode at concentration of 0.2 mg/L, this assembly domain has a thickness of ~3 nm and shows

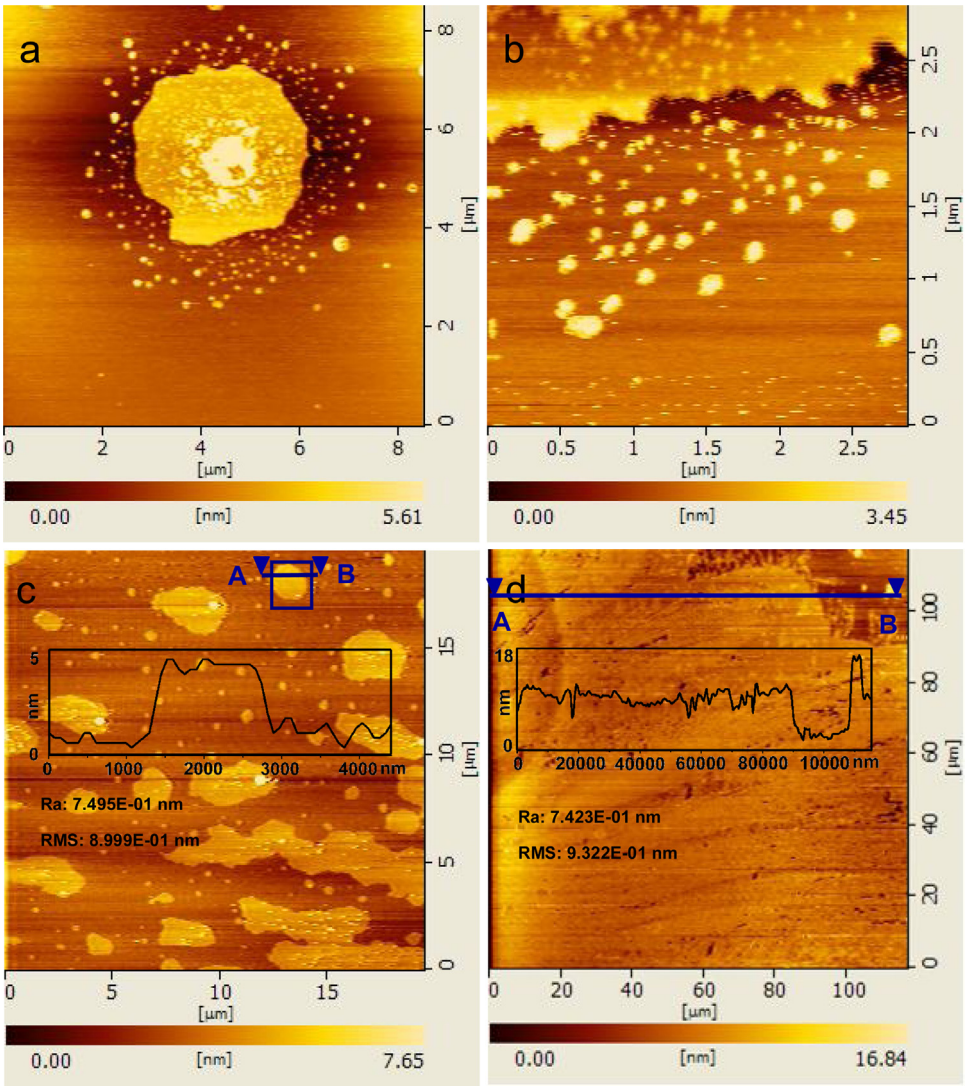

Fig. 3. (a) MTQDs aggregation in a layer-plus-island mode, (b) enlarged view of the edge of (a), (c) percolating network domain of MTQDs, and (d) continuous film self-assembled by MTQDs.

a smooth surface with a higher island at the center, indicating a layer-plus-island growth mode.

Increasing the colloid concentration to 1 mg/L, isolated assembly domains connect gradually with each other, the assembly morphology changes from isolated domains to percolating network domains. In this extension process, although the growth along in-plane direction is obvious, the increasing of thickness is limited (Fig. 3c).

Increasing the colloid concentration to 5 mg/L, MTQDs percolating network domains connect all together eventually to form a compact ultrathin film with thickness of several nanometers and a lateral dimension of up to hundreds of micrometers (which is the maximum scan area of the AFM instrument we used. Fig. 3d). Because all the isolated domains are connected with each other, the distinction between the "island center" and "island edge" which formed as a result of layer-plus-island growth mode become blurred. It is worth mentioning that the surface flatness of this ultrathin film is quite high, the values of Ra and RMS roughness are only 0.74 nm and 0.93 nm, respectively, indicating the assembly MTQDs film prepared by a simple drop-cast method is even smoother than the film fabricated by complex magnetron sputtering method.

Microscopic phenomenon of evaporation of MTQDs colloid show information more intuitively. Deposited on silicon substrate,

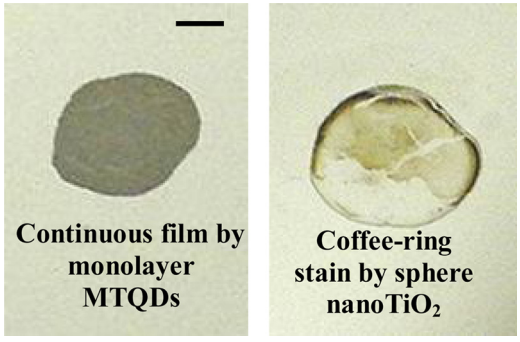

Fig. 4. Photograph of continuous film and coffee-ring stain left on a silicon substrate in the drop drying process by monolayer MTQDs and sphere nanoTiO_2 particles. Scale bar: 2 mm.

a drop of two-dimensional anisotropic plate-like MTQDs colloid left a uniform and continuous film after evaporation. By contrast, a drop of TiO_2 nanoparticle colloid with similar lateral size but a three-dimensional sphere shape left a typical coffee ring stain on the silicon substrate after the same evaporation procedure (Fig. 4).

To explain the self-assembly behavior observed in AFM detection and the coffee-ring suppression intuitively showed in

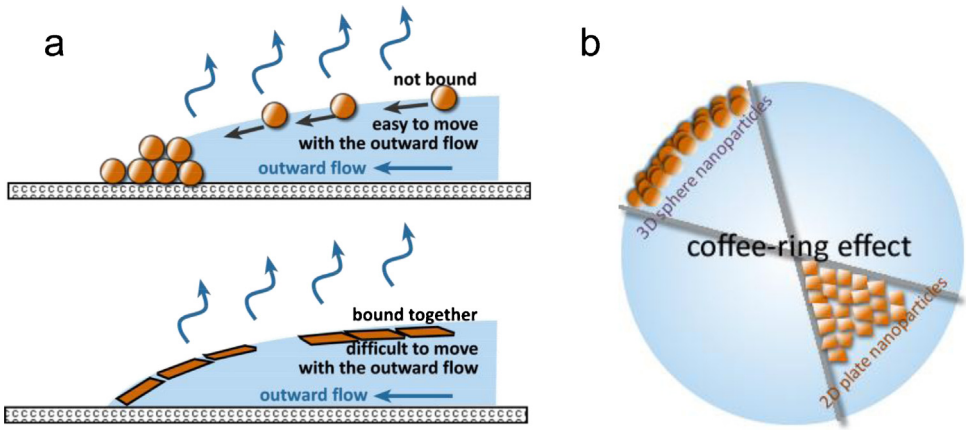

Fig. 5. Illustration of the differences between 3D sphere particles and 2D plate-like MTQDs in coffee-ring effect. (a) Side view and (b) top view.

microscope observation, the causes and mechanism of coffee ring effect should be considered. According to previous studies, two kinds of flow inside the droplet are considered as the main cause for the formation of coffee-ring deposit: An outward flow flowing from interior to exterior to replenish the liquid removed by evaporation at the edge of pinned contact line [23], and a Marangoni flow generated from nonuniform evaporation at the free surface of droplets [24]. The Marangoni flow, which can induce strong convection, is much more prominent in highly volatile solvents (e.g., octane, ethanol, and pentane) and can hardly be observed in aqueous solutions owing to the combination of relatively lower volatility and higher heat capacity of water [25,26]. In this experiments, because the solvent used is pure-water, the mitigation of outward flow, instead of Marangoni flow, should be the dominant factor for the suppression of coffee-ring effect.

A recent research reported that, the coffee-ring effect could be suppressed by using anisotropic ellipsoidal particles instead of common sphere particles [27]. That is because: (1) comparing with sphere particles, the interparticle attraction between anisotropic particles and the attraction between particles and interface are more than two orders of magnitude stronger; (2) owing to the strong interparticle attraction, the encountered anisotropic particles behave in a "stick-and-stay" manner. Because the energy cost for deforming, moving or breaking up the clusters is very large, once encountered, they tightly bind with each other and attach to the interface; (3) the mobility of these bound particles is markedly reduced and they resist the radially outward flow which mentioned above as one of the two main reasons for the forming of coffee ring effect. In our experiment, two-dimensional MTQDs with similar anisotropic morphology as ellipsoidal particles are used. These single layer quantum dots have not only a typical anisotropic shape, but also many unsaturated dangling bonds at the periphery, which would further enhance the binding between the particles/particles and the particles/interface. Moreover, because pure water is the only solvent used in the experiment, MTQDs are not covered with detergent or surfactant. This ligand-free feature of the MTQDs is also beneficial for the connection between the particles. Therefore, since the mitigation of outward flow is resisted by the firm connection between anisotropic MTQDs particles and the Marangoni flow is also mitigated by using pure water as solvent, coffee-ring effect is successfully suppressed and an ultrathin titania film was left after the evaporation of MTQDs colloid in our experiment (see Supplementary information for more detail of the self-assembly behavior in drying process, Fig. S1). On the contrary, to sphere nanoparticle colloid, because of weak interparticle attraction and relative "clean" particle surface, sphere particles cannot bound tightly with each other, and therefore cannot deform the interface and change the surface tension significantly. Thus, sphere particles are carried away by outward flow and stick at the pinned edge to form a coffee-ring stain (illustrated in Fig. 5a and b).

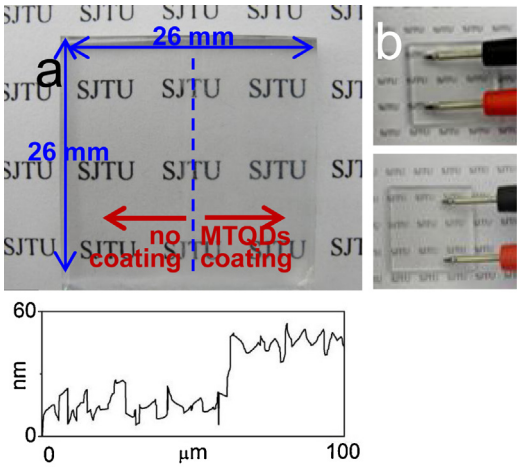

Fig. 6. (a) Photograph of ITO conductive glass without and with MTQDs coating. (b), (c) The resistant of ITO conductive glass increased from ~30 Ω to ~3 MΩ after MTQDs coating.

3.3. Photocatalytic performance of MTQDs and graphene/MTQDs

The suppression of coffee-ring effect is beneficial to form a high quality film in the spray coating method. In a controlled condition (90% ambient humidity, 10 °C), a continuous ultrathin titania film can be prepared by spray at room temperature. A simple but intuitive experiment was designed to demonstrate the continuity of the film. A MTQDs film with 30 nm around thickness was prepared by using spray method on an ITO-glass with good conductivity (Fig. 6 owing to the roughness of ITO-glass, the surface of MTQDs film was rougher than that in Fig. 3d). Because any uncovered surface of conductive glass can be used by electrons to form a conductive path, the resistivity will hardly increase if the MTQDs coating is not dense and continuous. Such dense and continuous titania film with a thickness of only several tens of nanometers is almost impossible to fabricate by using a simple spray method at room temperature, however, the ultrathin morphology of MTQDs and the suppression of coffee-ring effect raise the possibility. In our experiment, compared with uncovered ITO-glass, the resistivity increased significantly from ~30 Ω to ~3 MΩ (Fig. 6) after MTQDs coating, indicating an excellent continuity of the spray coating film.

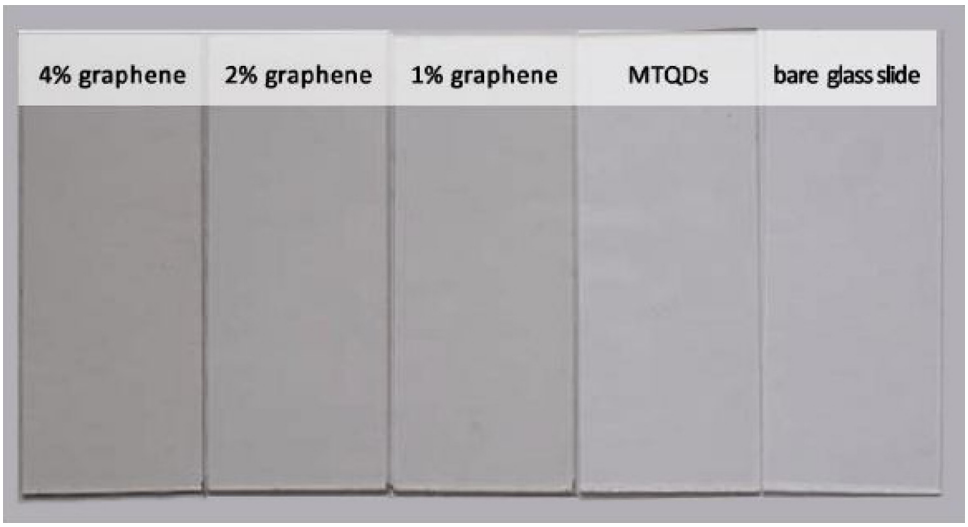

Fig. 7. Photograph of MTQDs/graphene composite films deposited on glass slides by spray coating method with different graphene loading amount.

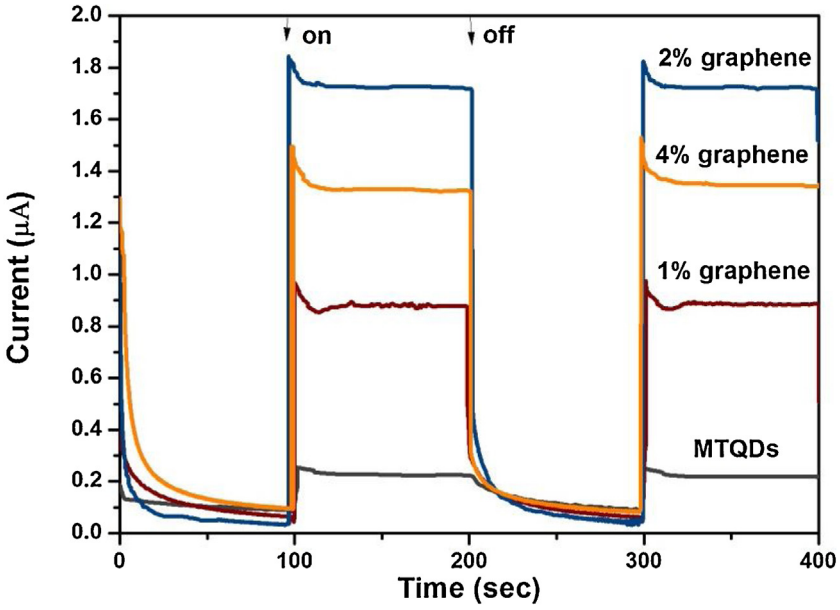

Fig. 8. Transient photocurrents of MTQDs and MTQDs/graphene films under 350 W Xe-lamp (without bias voltage).

The photocatalytic performance of MTQDs was detected by the degradation of MB dye in solution under the irradiation of UV light. Photocatalytic performance experiments demonstrated that the photocatalytic activity of MTQDs particle is lower than that of P25 (because it is difficult to prepare a P25 film under room temperature, the comparison is made between the particles instead of films, see Supplementary information Fig. S2). The lack of internal crystal structure along *z*-direction may hinder the transfer of photoinduced electrons and, therefore, reduce the photocatalytic activity of MTQDs. To improve the activity of MTQDs, graphene loading is employed in our experiments. Many researches have confirmed the promotion of graphene on TiO_2 photocatalysis performance by enhancing the separation of photo-induced electron/hole pairs. But owing to the covalent bonding or non-covalent anchoring of TiO_2 on paper-like graphene substrate, the particle size of the composites is generally large, making it difficult to obtain a stable composite suspension, and therefore hindering the preparation of ultrathin graphene/TiO_2 composite films. In our experiments, stable MTQDs/graphene composite colloids with different graphene loading amount are synthesized and their corresponding films are deposited on glass substrates by spray coating method (Fig. 7). The result of film transient photocurrents test, showed in Fig. 8, indicated that an obvious improvement of MTQDs photoelectric conversion efficiency is obtained by loading graphene. The results of photocatalytic performances of MTQDs and its composite particles are consistent with the transient photocurrents test and also demonstrate that after graphene loading, the activity of the

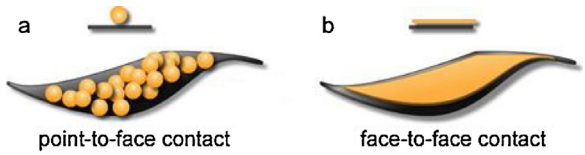

Fig. 9. Spherical particles contact with two-dimensional graphene in a point-to-face way. Flake-like particles contact with graphene in a face-to-face manner, which would increase the effective contact area between them.

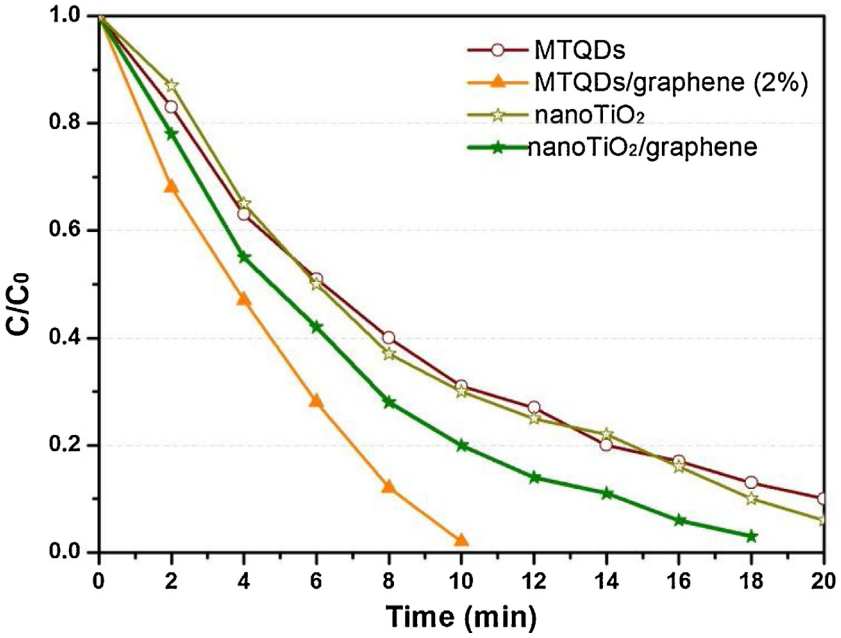

Fig. 10. Photocatalytic degradation of MB by films of MTQDs, MTQDs/graphene, nanoTiO_2 nanoTiO_2/graphene.

graphene/MTQDs composites is higher than that of P25 (Supplementary information, Fig. S3).

Owing to the sphere shape of TiO_2 particles and the paper-like shape of graphene, the contact between them with either covalent or non-covalent bonding is generally in a point-plane mode, giving a limited contact area (Fig. 9a). This will obviously suppress the electronic transfer, and reduce the enhancement of photocatalytic activity. In our previous study, it was demonstrated that MTQDs have the tendency to in-plane spread on carbon film which coating on the TEM grid or on HOPG which served as substrate for STM detection [8]. Therefore, although the combination between graphene and MTQDs is difficult to clearly observe owing to the mismatching in size, it is rational to infer that MTQDs will also in-plane spread on graphene with a face-to-face contact mode (Fig. 9b). To examine whether the contact mode (point-face or face-face) has influence to the electron–hole separation efficiency of graphene, photocatalytic performances of sphere-shape nanoTiO_2, and nanoTiO_2/graphene composite are detected for comparison. The nanoTiO_2 particles are spherical particles with a diameter around 2–5 nm (please see our previous paper [13] for the information of characteristics and film formation in detail). Experiment results demonstrated that (Fig. 10), sphere-shape nanoTiO_2 particle has a similar photocatalytic activity to that of MTQDs. After loading the same amount of graphene, the activity of nanoTiO_2/graphene is lower than that of MTQDs/graphene. In considering the different contact mode of MTQDs/graphene and nanoTiO_2/graphene, the more efficiency promotion may be derived from the larger contact area between graphene and MTQDs.

4. Conclusions

In our research, the self-assembly behavior of two-dimensional MTQDs was microscopically examined by AFM. Since the mitigation of outward flow is resisted by the firm connection between anisotropic MTQDs particles and the Marangoni flow is also mitigated by using pure water as solvent, coffee-ring effect is successfully suppressed during the evaporation of MTQDs colloid. It is also confirmed that graphene loading can significantly improve the photocatalytic efficiency of MTQDs, this is not only due to the efficiency enhancement of photo-induced electron/hole pairs, but also due to the face-to-face contact mode between MTQDs and graphene. Therefore, a novel way is proposed in this paper to prepare an ultrathin transparent photocatalytic film with high efficiency using simple drop-cast or spray coating method at room temperature.

Acknowledgments

We gratefully acknowledge financial support by the National Key Basic Research and Development Program (Grant No. 2009CB220000), the National Natural Science Foundation of China (20973110), and the equipment support from Instrumental Analysis Center of Shanghai Jiao Tong University.

Appendix A. Supplementary data

Supplementary data associated with this article can be found, in the online version, at http://dx.doi.org/10.1016/j.apcatb.2015.06.049

References

[1] C. Garzella, E. Comini, E. Tempesti, C. Frigeri, G. Sberveglieri, Sens. Actuators B: Chem. 68 (2000) 189–196.
[2] N. Arconada, A. Durán, S. Suárez, R. Portela, J.M. Coronado, B. Sánchez, Y. Castro, Appl. Catal. B: Environ. 86 (2009) 1–7.
[3] S.D. Burnside, V. Shklover, C. Barbé, P. Comte, F. Arendse, K. Brooks, M. Grätzel, Chem. Mater. 10 (1998) 2419–2425.
[4] C. Garzella, E. Comini, E. Tempesti, C. Frigeri, G. Sberveglieri, Sens. Actuators B: Chem. 68 (2000) 189–196.
[5] D. Dumitriu, A. Bally, C. Ballif, P. Hones, P. Schmid, R. Sanjines, F. Levy, V. Parvulescu, Appl. Catal. B: Environ. 25 (2000) 83–92.
[6] M. Okuya, K. Nakade, S. Kaneko, Sol. Energy Mater. Sol. Cells 70 (2002) 425–435.
[7] S. Nakade, M. Matsuda, S. Kambe, Y. Saito, T. Kitamura, T. Sakata, Y. Wada, H. Mori, S. Yanagida, J. Phys. Chem. B 106 (2002) 10004–10010.
[8] H. Gao, G. Hu, W. Shangguan, K. Zhu, J. Supercrit. Fluids 88 (2014) 126–133.
[9] B.D. Yao, Y.F. Chan, X.Y. Zhang, W.F. Zhang, Z.Y. Yang, N. Wang, Appl. Phys. Lett. 82 (2003) 281–283.
[10] T. Kasuga, M. Hiramatsu, A. Hoson, T. Sekino, K. Niihara, Langmuir 14 (1998) 3160–3163.
[11] K. Zhu, H. Gao, G. Hu, Z. Shi, J. Supercrit. Fluids 83 (2013) 28–34.
[12] C. Liu, G. Hu, H. Gao, J. Supercrit. Fluids 63 (2012) 99–104.
[13] H. Gao, W. Chen, J. Yuan, Z. Jiang, G. Hu, W. Shangguan, Y. Sun, J. Su, RSC Adv. 3 (2013) 8559–8564.

[14] P. Kritzer, J. Supercrit. Fluids 29 (2004) 1–29.
[15] P.E. Savage, J. Supercrit. Fluids 47 (2009) 407–414.
[16] A. Kruse, E. Dinjus, Zeitschrift für Physikalische Chemie 219 (2005) 341–366.
[17] K. Fukuda, Y. Ebina, T. Shibata, T. Aizawa, I. Nakai, T. Sasaki, J. Am. Chem. Soc. 129 (2006) 202–209.
[18] K. Akatsuka, M.-A. Haga, Y. Ebina, M. Osada, K. Fukuda, T. Sasaki, ACS Nano 3 (2009) 1097–1106.
[19] M. Osada, T. Sasaki, J. Mater. Chem. 19 (2009) 2503–2511.
[20] D. Szieberth, A.M. Ferrari, Y. Noel, M. Ferrabone, Nanoscale 2 (2010) 81–89.
[21] T. He, M. Zhao, X. Zhang, H. Zhang, Z. Wang, Z. Xi, X. Liu, S. Yan, Y. Xia, L. Mei, J. Phys. Chem. C 113 (2009) 13610–13615.
[22] J.M. Hughes, Y. Hernandez, D. Aherne, L. Doessel, K. Müllen, B. Moreton, T.W. White, C. Partridge, G. Costantini, A. Shmeliov, M. Shannon, V. Nicolosi, J.N. Coleman, J. Am. Chem. Soc. 134 (2012) 12168–12179.
[23] R.D. Deegan, O. Bakajin, T.F. Dupont, G. Huber, S.R. Nagel, T.A. Witten, Nature 389 (1997) 827–829.
[24] H. Hu, R.G. Larson, J. Phys. Chem. B 110 (2006) 7090–7094.
[25] M. Majumder, C.S. Rendall, J.A. Eukel, J.Y.L. Wang, N. Behabtu, C.L. Pint, T.-Y. Liu, A.W. Orbaek, F. Mirri, J. Nam, A.R. Barron, R.H. Hauge, H.K. Schmidt, M. Pasquali, J. Phys. Chem. B 116 (2012) 6536–6542.
[26] X. Xu, J. Luo, Appl. Phys. Lett. 91 (2007) 124102–124103.
[27] P.J. Yunker, T. Still, M.A. Lohr, A.G. Yodh, Nature 476 (2011) 308–311.